Research Article

Chu Cheng, Kexing Song*, Xujun Mi, Baoan Wu, Zhu Xiao, Haofeng Xie, Yanjun Zhou, Xiuhua Guo, Haitao Liu, Dingbiao Chen, Xiaoyu Shen, and Yong Ding

Microstructural evolution and properties of Cu–20 wt% Ag alloy wire by multi-pass continuous drawing

https://doi.org/10.1515/ntrev-2020-0108
received November 26, 2020; accepted December 9, 2020

Abstract: The Cu–20 wt% Ag alloy wire rod was prepared using three-chamber vacuum cold mold vertical continuous up-casting followed by multi-pass continuous drawing. The evolution of microstructure, mechanical property, and electrical property of the Cu–20 wt% Ag alloy wire during multi-pass continuous drawing was studied. After multi-pass continuous drawing, the continuous network eutectic structure in the longitudinal section of the as-casted rod was gradually drawn into long fibers that approximately parallel to the axial direction, while the space of the continuous network eutectic structure in the transverse section is getting smaller and smaller. Both the preferred orientation of copper and silver grains are (1,1,1). With the increase of drawing strain (η), the tensile strength of Cu–20 wt% Ag alloy wire gradually increases while the elongation gradually decreases. When the diameter is drawn to 0.02 mm (η = 11.94), the tensile strength of the alloy is 1,682 MPa and elongation is 2.0%. The relationship between tensile strength, elongation, and diameter conforms to Allometric and Boltzmann functions, respectively.

Keywords: Cu–Ag alloy, multi-pass continuous drawing, microstructure evolution, mechanical property, electrical property

*** Corresponding author: Kexing Song,** School of Materials Science and Engineering, Henan University of Science and Technology, Luoyang 471023, China; Provincial and Ministerial Co-construction Collaborative Innovation Center of Nonferrous New Materials and Advanced Processing Technology, Luoyang 471023, China; Henan Key Laboratory of Advanced Non-Ferrous of Metals, Luoyang 471023, China, e-mail: kxsong@haust.edu.cn
Chu Cheng: School of Materials Science and Engineering, Henan University of Science and Technology, Luoyang 471023, China; Provincial and Ministerial Co-construction Collaborative Innovation Center of Nonferrous New Materials and Advanced Processing Technology, Luoyang 471023, China; Henan Key Laboratory of Advanced Non-Ferrous of Metals, Luoyang 471023, China, e-mail: cheng_chu_love@126.com
Xujun Mi: GRIMAT Engineering Institute Co., Ltd, State Key Lab Nonferrous Met & Proc, Beijing 101417, China, e-mail: mxj@grinm.com
Baoan Wu: Chongqing Materials Research Institute, Co., Ltd., Functional Materials Research Institute, Chongqing 400707, China, e-mail: wubaoan@163.com
Zhu Xiao: School of Materials Science and Engineering, Central South University, Changsha 410083, China, e-mail: xiaozhumse@163.com
Haofeng Xie: GRIMAT Engineering Institute Co., Ltd, State Key Lab Nonferrous Met & Proc, Beijing 101417, China, e-mail: xiehaofeng@grinm.com
Yanjun Zhou: School of Materials Science and Engineering, Henan University of Science and Technology, Luoyang 471023, China; Provincial and Ministerial Co-construction Collaborative Innovation Center of Nonferrous New Materials and Advanced Processing Technology, Luoyang 471023, China; Henan Key Laboratory of Advanced Non-Ferrous of Metals, Luoyang 471023, China, e-mail: dazhou456@163.com
Xiuhua Guo: School of Materials Science and Engineering, Henan University of Science and Technology, Luoyang 471023, China; Provincial and Ministerial Co-construction Collaborative Innovation Center of Nonferrous New Materials and Advanced Processing Technology, Luoyang 471023, China; Henan Key Laboratory of Advanced Non-Ferrous of Metals, Luoyang 471023, China, e-mail: guoxiuhua@sina.com
Haitao Liu: School of Materials Science and Engineering, Henan University of Science and Technology, Luoyang 471023, China; Provincial and Ministerial Co-construction Collaborative Innovation Center of Nonferrous New Materials and Advanced Processing Technology, Luoyang 471023, China; Henan Key Laboratory of Advanced Non-Ferrous of Metals, Luoyang 471023, China, e-mail: htliu1204@163.com
Dingbiao Chen: Changzhou Hengfeng Special Conductor Co. Ltd, Changzhou, 213000, China, e-mail: cheng_chu_love@126.com
Xiaoyu Shen: Zhejiang Tony Electronic Co., Ltd, Huzhou, 313000, China, e-mail: yaoyushen@tony-tech.com
Yong Ding: Zhejiang Tony Electronic Co., Ltd, Huzhou, 313000, China, e-mail: diego.ding@tony-tech.com

1 Introduction

Copper alloy and copper matrix composite materials have many advantages of good arc erosion corrosion resistance [1], wear resistance [2], high strength [3], and other special properties [4]. Due to the excellent strength and high conductivity of Cu–Ag alloy, they are widely used as bonding wire in high-end fields such as integrated circuit packaging, connector [5], electronic communication [6], and audio and video transmission [7]. At present, the Cu–Ag alloy mainly contains low-silver and high-silver alloy wire according to the silver content [8]. Cu–Ag alloy wire with silver content of 0.06–0.3 wt% is widely used as contact wire and data wire [9]. It can replace pure copper as data wire because it has a higher strength, and at the same time, its processing characteristics are the same as those of pure copper wire [10]. The Cu–Ag alloy wire with silver content of 1–20 wt% mainly includes Cu–1 wt% Ag, Cu–2 wt% Ag, Cu–3 wt% Ag, Cu–4 wt% Ag, Cu–6 wt% Ag, Cu–10 wt% Ag, and Cu–20 wt% Ag. Cu–Ag alloy wire with silver content of 1–6 wt% is widely used as voice coil, flexible cables, and bending resistance cable in the field of automotive, medical, and smart devices [11]. When the silver content is more than 10.0 wt%, the Cu–Ag alloy wire is often used as conductive material in splice pieces and precise resistance [12].

The traditional method to prepare Cu–Ag alloy wire is cold mold continuous casting, followed by multi-pass drawing and intermediate annealing [13]. The obtained materials by this mature method usually present good stability [14]. However, segregation and defects always can be observed when we prepared Cu–Ag alloy with high Ag content because of wide solidification range, which leads to breaking during the subsequent drawing process [15]. As a result, super long and slim Cu–Ag alloy wire with high Ag content is difficult to be prepared [16,17]. At present, many researchers in the world are working on the preparation technology of Cu–Ag alloy wire [18]. Feng *et al.* [19] have studied the influence of drawing process on the performance of directional solidified Cu–Ag alloy wire. The result shows that Cu–Ag alloy wire with the diameter of 0.12 mm can be prepared through the horizontal continuous solidification, followed by multiple cold drawing. The electrical conductivity of the material is up to 58.0 MS/m, with a tensile strength of 300 MPa and elongation of 23%. Ning *et al.* [20] have researched the preparation of Cu–10Ag *in situ* nanofiber composite by large deformation, and the results show that the tensile strength of the Cu–Ag alloy wire is up to 1,190 MPa and the conductivity is 68.7% IACS. Zhang *et al.* [21,22] and Konakov *et al.* [23] have studied the effects of fiber phase and alloying elements on the microstructure, mechanical properties, and electrical properties of Cu–Ag alloy wire. The result shows that when the eutectic fiber bundle space is more than 150 nm, the relationship between tensile strength and the eutectic fiber bundle space is consistent with Hall–Pecth, and the strengthening effect is considered to be the dislocation plug mechanism [24]. For the as-casted Cu–Ag alloy with low Ag content, few second phases were draw into loosely arranged fibers after cold drawing, which loosely distributed in the copper dendrite gap [25]. However, for the alloy with high Ag content, second phases in the microstructure exist in the form of reticular continuous eutectic layer, and the fibers were arranged in a straight and dense manner after cold drawing. Zuo *et al.* [26] and Zhao *et al.* [27] have studied the microstructure and properties of nanostructured Cu–28 wt% Ag microcomposite deformed after solidifying under a high magnetic field. The result shows that the strength of Cu–Ag alloy composites solidified under a high magnetic field is significantly improved due to the smaller space of silver eutectic tissue. Previous research work reported by Liu *et al.* [28] evaluated the evolution of microstructure and properties of Cu–Ag microcomposites with different Ag content. They found that the increased deformation may lead to the improved tensile strength and decreased electrical conductivity of Cu–Ag alloy. The morphology of eutectic microstructure of Cu–24 wt% Ag alloy has a greater influence on the strength and conductivity than its volume fraction.

In this paper, Cu–20 wt% Ag alloy wire was prepared through three-chamber vacuum and cold mold vertical continuous up-casting followed by multi-pass continuous drawing [29]. The effect of drawing process on the microstructure, texture, mechanical properties, and electrical performance of Cu–20 wt% Ag alloy wire was systematically studied. This study will provide theoretical basis for the superfine, continuous, and accurate drawing control of Cu–Ag alloy with high Ag content.

2 Experiment

2.1 Experimental process

The as-cast Cu–20Ag rod was prepared by self-developed three-chamber vacuum and cold mold vertical continuous up-casting equipment, as shown in Figure 1. Electrolytic copper (99.95%) and high-purity silver particles

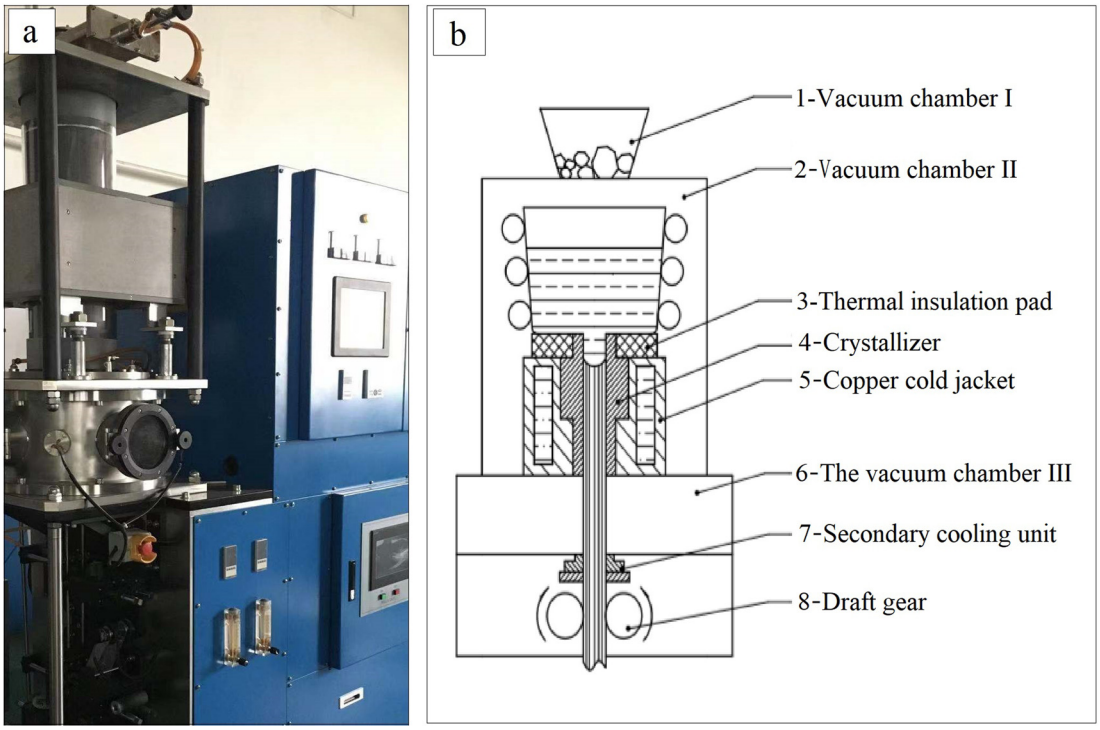

Figure 1: Three-chamber vacuum cold mold vertical drawing continuous casting device (a) and its schematic diagram (b).

(99.99%) were used as raw materials. They were placed with a mass proportion of 4:1 in vacuum chamber I. After that, the vacuum chamber I was vacuumed. Secondly, they were smelted in an intermediate frequency induction furnace (≤2,000 Hz) in vacuum chamber II [30]. Thirdly, the as-cast Cu–20Ag rod with a diameter (Φ) of 7.83 mm was prepared from casting mold with a speed of 150 mm/min by cooling after they were fully mixed [31]. Finally, the as-cast Cu–20Ag rod was continuously cold drawn from Φ 7.83 mm to Φ 0.02 mm. Then the materials were heated at 550°C for 1 s. The drawing strain is calculated by $\eta = \ln(A_0/A)$, where A_0 and A are initial and final cross-sectional areas, respectively. The total drawing strain η is 11.94.

2.2 Analysis methods

The longitudinal and transverse samples were taken from as-cast rod and as-drawn wire with different diameters during multi-pass continuous drawing. After the surface is polished and corroded, the samples were etched using the mixture solution containing 30% $NH_3{\cdot}H_2O$ and 20% H_2O_2 (vol% 1:1). The microstructure was analyzed using a Zeiss AxioVert A1 optical microscope and a field-emission scanning electron microscope (FE-SEM, JSM-7800F, JEOL, Japan). The texture was analyzed using a X-Ray Diffraction (Model D8 Bruker, Germany) with a Cu Kα1 source at 40 kV and 40 mA. Tensile mechanical tests were carried out using a AG-I250KN electronic universal materials testing machine at room temperature. The electrical conductivity were measured using ZY9987 electrical conductivity gauge.

3 Results and discussion

3.1 Microstructure and texture

Figure 2 shows the longitudinal macrophotograph, longitudinal and transverse microstructure of as-cast rod, and as-drawn wire during multi-pass continuous drawing.

As shown in Figure 2b, the longitudinal microstructure of as-cast rod prepared using three-chamber vacuum cold mold vertical continuous up-casting consists of two components: Cu-rich proeutectic matrix (dark contrasts) and Ag-rich eutectic dendrite (light contrasts), which form a rhombic network along the axial direction [32].

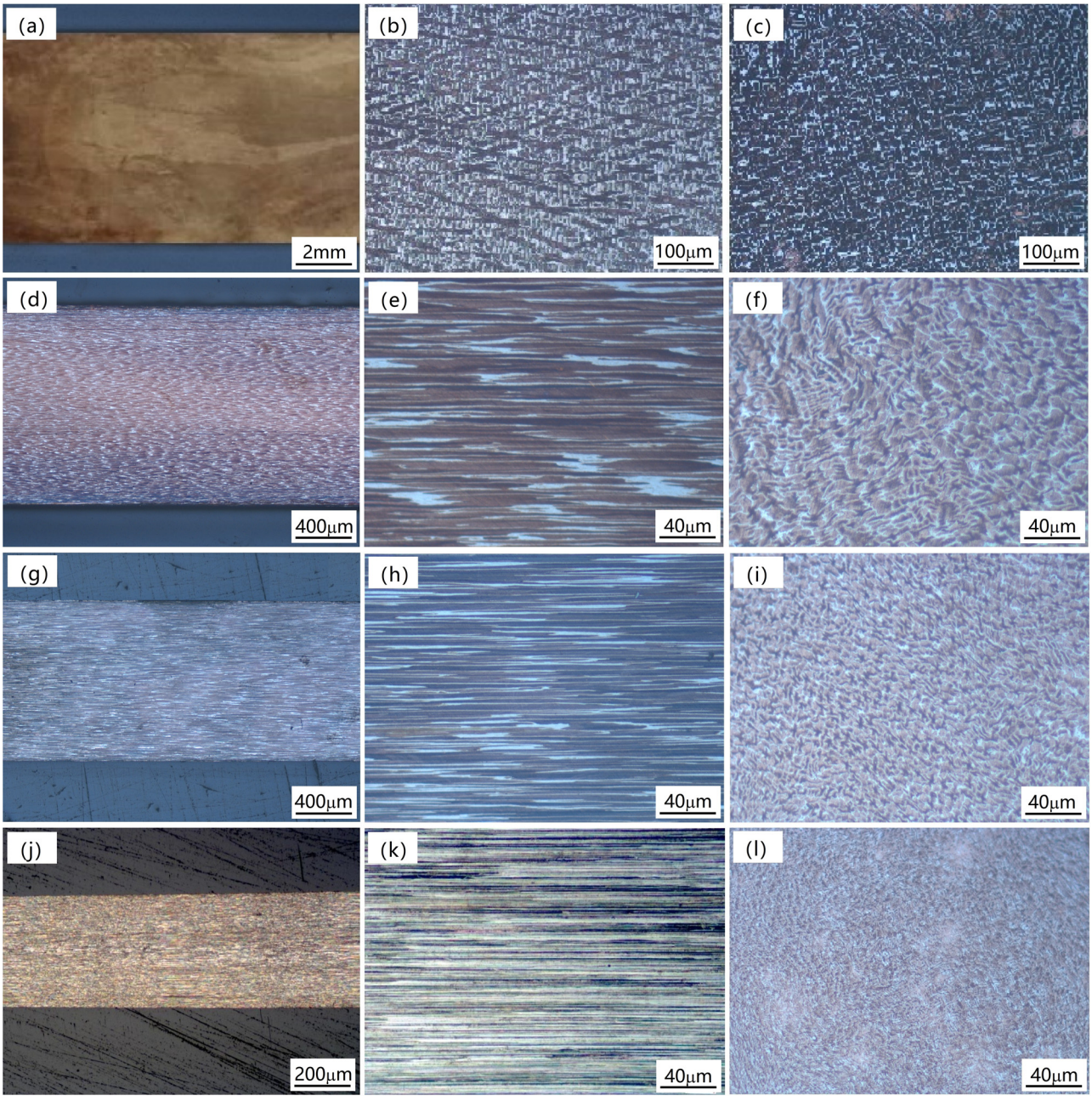

Figure 2: The longitudinal macrophotograph, longitudinal, and transverse microstructure of as-cast rod and as-drawn wire with different diameters (a–c – 7.83 mm, η = 0; d–f – 2.13 mm, η = 2.6; g–i – 1.00 mm, η = 4.1; j–l – 0.45 mm, η = 5.7).

Compared with Figure 2e, h, and k, the continuous network eutectic structure in the longitudinal section of the as-cast rod is gradually drawn into long fibers during multi-pass continuous drawing. Those fibers are approximately completely parallel to the axial direction as a function of drawing strain and its space is getting smaller and smaller [33]. In addition, longitudinal macrophotographs in Figure 2a, d, g, and j show that the space of the peripheral fibers is much smaller than that of the core, indicating that the deformation of the periphery in the wire is significantly greater than that of the core during multi-pass continuous drawing [34]. What is more, the deformation gradually weakens from the circumference to the core along the diameter direction. This is mainly due to the deformation process during the drawing: the metal of the periphery in the wire first deforms as a result of shear force when the wire goes across the obconical mould, and then grains in the center slip being motivated

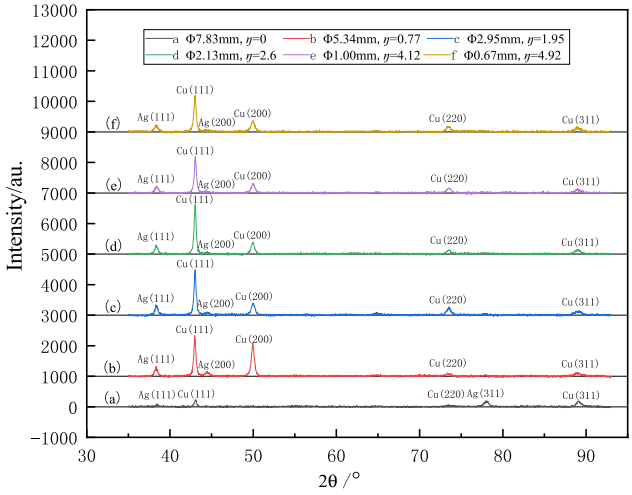

Figure 3: XRD patterns of as-cast rod and as-drawn wire with different diameters during multi-pass continuous drawing (a – as-cast; b–f – as-drawn).

by the deformation of the periphery. As a result, the deformation of the periphery in the wire is significantly greater than that of the core during multi-pass continuous drawing [35]. Figure 2c shows that the transverse microstructure of as-cast rod is composed of Cu-rich proeutectic matrix and Ag-rich eutectic dendrite, which form a ruleless network. Compared with Figure 2f, i, and l, after multi-pass continuous drawing, they are still ruleless network in the transverse microstructure, but the space is getting smaller and smaller and the microstructure is getting more dense [36]. In conclusion, after multi-pass continuous drawing, the continuous network eutectic structure in the longitudinal section of the as-cast rod is gradually drawn into long fibers which are approximately parallel to the axial direction, while the cross section is gradually drawn into ruleless network with a smaller space.

Figure 3 shows XRD patterns of as-casted rod and as-drawn wire with different diameters after multi-pass continuous drawing. Three diffraction peaks of Cu(111), Cu (220), and Cu(311) and two diffraction peaks of Ag(111) and Ag(311) can be observed in the as-casted rod prepared using three-chamber vacuum cold mold vertical continuous up-casting. The intensity of Cu(111) and Cu (311) diffraction peaks is stronger than that of Cu(220), and Ag(311) is stronger than that of Ag(111). This is mainly determined by in-house crystal structure and the parameters of vertical continuous up-casting. During multi-pass continuous drawing, the intensity of diffraction peak Cu(111) increases. At the same time, the diffraction peak of Cu(200) can be observed, the intensity of which weakened with the decrease of diameter. The diffraction peak of Cu(220) was weak in the as-cast rod and the wire with a diameter of 5.34 mm, but it increases when the diameter of the wire is drawn to 2.95 mm, indicating that the process is conducive to the growth of Cu(220) and the volume fraction of Cu(220) increases in its structure. Then, its intensity weakens with the decreasing diameter. However, the intensity of Cu(311) peak changed a little during multi-pass continuous drawing. The intensity of Ag(111) peak increases after drawing, and the intensity without obvious difference with the decreased diameter. At the same time, the diffraction peak of Ag(200) arises, and its intensity decreases with the decreased diameter. In addition, the diffraction peaks of Ag(311) gradually disappear, indicating that the volume fraction of Cu (311) gradually decreases. It can be concluded that, after multi-pass continuous drawing, the slip plane and the slip direction of each grain in the Cu–20 wt% Ag wire turn toward the direction of drawing as a function of drawing strain, resulting in the formation of organized grain orientation. The strongest peak is Cu(111) and the preferred orientation of copper grains is (1,1,1) [37]. The intensity of Ag(111) peak is the highest and the preferred orientation of silver grains is (1,1,1).

3.2 Mechanical properties

Figure 4 shows the tensile strength and elongation of alloy wires with different diameters during multi-pass continuous drawing.

Figure 4 shows the tensile strength and elongation of alloy wires with different diameters during multi-pass continuous drawing. The rod prepared using three-

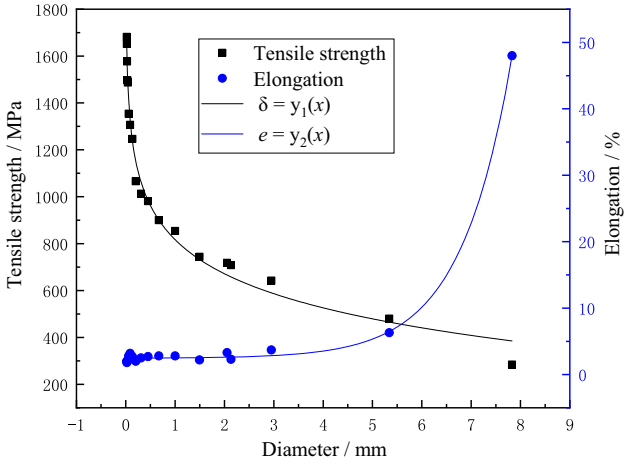

Figure 4: Mechanical properties of as-drawn wires with different diameters during multi-pass continuous drawing.

chamber vacuum cold moertical continuous up-casting presents excellent plasticity, with a tensile strength of 284 MPa and elongation of 48.0%. During the multi-pass continuous drawing, its tensile strength increases gradually with the decrease of diameter [38]. The tensile strength continuously increases when the diameter of alloy wires is drawn from 7.83 to 1.00 mm (η = 4.12). When the diameter is drawn from 1.00 to 0.02 mm (η = 11.94), the tensile strength of alloy wires gradually increases to 1,682 MPa. This is mainly attributed to the fact that the continuous network eutectic structure in the longitudinal section is gradually drawn into long fibers through multi-pass continuous drawing, which are approximately parallel to the axial direction. Meanwhile, work-hardening occurs as the function of drawing strain, which leads to a gradual increase of the tensile strength[39]. However, the elongation of the Cu–20 wt% Ag alloy wire is closely related to the diameter, which decreases rapidly from 48% to 3.68% when the diameter of alloy wires is drawn from 7.83 to 2.95 mm (η = 1.95) due to the sharp increase of the dislocation density inside the grains after drawing deformation [40]. When the diameter is gradually drawn from 2.13 mm (η = 2.60) to 0.02 mm, the elongation of Cu–20 wt% Ag alloy wire tends to be stable at a range of 1.8–3.3%. This is mainly attributed to the fact that the silver fibers have been approximately parallel to the axial direction with a diameter less than 2.13 mm [41].

In order to further research the relationship between the diameter and mechanical properties of Cu–20 wt% Ag alloy wires during multi-pass continuous drawing, Allometric and Boltzmann functions were used to fit the data of the tensile strength and elongation of the alloy wires, respectively. The fitting results were shown in Figure 4. The relationship for tensile strength (δ), elongation (e), and diameter (x) is shown as the following equation:

$$\delta = 178285.85 - 177468.84 \times x^{0.00118} \tag{1}$$

$$e = (5437.56257 - 5435.11958)/(1 + \exp(x - 12.71763/\mathrm{d}x)) \tag{2}$$

The correlation coefficients between tensile strength (δ), elongation (e), and diameter (x) are calculated as 0.98656 and 0.99763, respectively, indicating that the fitting results are highly reliable.

Figure 5 shows the fracture morphology of the as-casted rod and as-drawn wire with different diameters during multi-pass continuous drawing. Significant differences can be found for the fracture dimples with different diameters. Numerous dimples with large size and deep depth can be observed on the as-casted rod fracture,

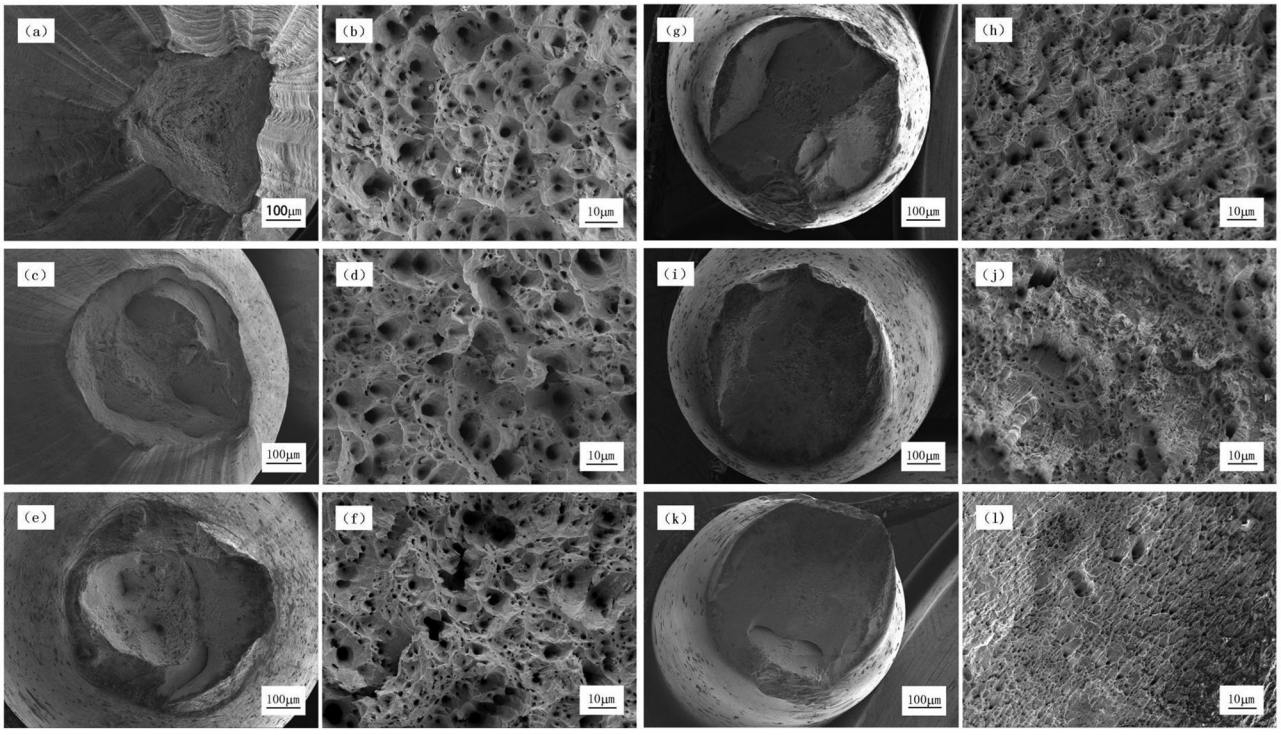

Figure 5: Fracture morphology of as-cast rod and as-drawn wire with different diameters (a and b – 7.83 mm, η = 0; c and d – 5.34 mm, η = 0.77; e and f – 2.95 mm, η = 1.95; g and h – 2.13 mm, η = 2.6; k and l – 1.49 mm, η = 3.31).

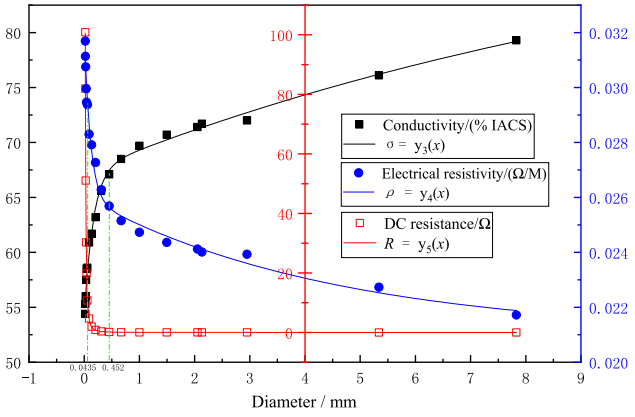

Figure 6: Electrical properties of as-drawn wires with different diameters during multi-pass continuous drawing.

presenting apparent necking phenomenon, which belongs to a typical ductile fracture. With the increase of the drawing strain, the necking phenomenon of the fracture becomes weaker, especially when the diameter is less than 2.13 mm (η = 2.6), the fracture almost tends to be flat. In addition, the number, depth, and size of the fracture dimples gradually become smaller and more uniform, which indicates that the microstructure of the alloy wire has been refined and its structure is more and more uniform through the deformation in the process of multi-pass continuous drawing. In addition, the tensile strength of the material is significantly improved, and the plasticity is greatly reduced, which is in accordance with the change rule of tensile strength and elongation in Figure 4.

3.3 Electrical properties

Figure 6 shows the conductivity, DC resistance, and electrical resistivity of Cu–20 wt% Ag alloy wires with different diameters during multi-pass continuous drawing.

It can be seen that the conductivity, resistivity, and DC resistance for the as-casted rod obtained by vacuum cold mold vertical continuous up-casting are 79.30% IACS, 2.17 × 10^{-2} Ω/M, and 4.51 × 10^{-4} Ω, respectively. During multi-pass continuous drawing, with the decrease of the diameter (the drawing strain increases, namely), the conductivity of alloy wires gradually decreases, while the electrical resistivity and DC resistance gradually increase [42]. When the diameter of the alloy wire is drawn from 7.83 mm (η = 0) to 0.452 mm (η = 5.70), its conductivity gradually decreases, while electrical resistivity gradually increases and the DC resistance slightly increases. When the diameter of the alloy wire is drawn from 0.452 to 0.0435 mm (η = 10.39), the conductivity rapidly decreases, while the electrical resistivity and DC resistance both rapidly increase. When the diameter of the alloy wire is gradually drawn from 0.0435 to 0.02 mm (η = 11.94), the conductivity rapidly decreases, while the electrical resistivity and DC resistivity sharply increase. Meanwhile, when the diameter of the alloy wire is gradually drawn from 0.435 to 0.02 mm, its conductivity drops sharply from 58.5% IACS to 54.4% IACS, electrical resistivity increases greatly from 2.95 × 10^{-2} to 3.17 × 10^{-2} Ω/M, and the DC resistance increases sharply from 19.82 to 100.88 Ω. This is mainly attributed to that, as the drawing proceeds, crystal defects such as microscopic cracks, inter-space, lattice defects, and dislocations are generated in the intragranular [43]. These defects will accumulate as the amount of deformation increases, resulting in the increase of the electrical resistance and decrease of the conductivity [44]. On the other hand, compared to the microstructure in Figure 2, it can be noticed that the average distance of the fibrous structure gradually becomes smaller, and the interface scattering increases with the decrease of distance of the fibers, which will cause the increase of the electrical resistivity and the decrease of the conductivity simultaneously [45].

In order to further research the relationship between the diameter and electrical properties of Cu–20 wt% Ag alloy wires during multi-pass continuous drawing, ExpAssoc and Allometric functions were used to fit the data of conductivity, DC resistance, and electrical resistivity of the alloy wires, respectively. The curves in Figure 6 are the fitting results. The conductivity (σ), electrical resistivity (ρ), and DC resistance (R), respectively, satisfy the following equation:

$$\sigma = 54.14533 + 13.22378 \times (1 - \exp(-x/0.16254)) + 25.25106 \times (1 - \exp(-x/12.39722)) \quad (3)$$

$$\rho = 0.03204 - 0.00499 \times (1 - \exp(-x/4.49466)) - 0.00603 \times (1 - \exp(-x/0.11232)) \quad (4)$$

$$R = 0.02852 \times x^{-2.08785} \quad (5)$$

The correlation coefficients between conductivity (σ), electrical resistivity (ρ), and DC resistance (R) and diameter (x) are, respectively, calculated as 0.9907, 0.9857, and 0.9997, indicating that the fitting results are highly reliable.

4 Conclusions

During the multi-pass continuous drawing process, the continuous network eutectic structure in the longitudinal

section of the as-casted Cu–20 wt% Ag rod is gradually drawn into long fibers that approximately parallel to the axial direction. However, the space of the continuous network eutectic structure in the transverse section became much more smaller. The obtained wire present typical (1,1,1) face-centered cubic structure. With the increase of drawing strain, the tensile strength of Cu–20 wt% Ag alloy wire appeared an increasing trend, while the elongation showed an opposite character. The relationship between tensile strength, elongation, and its diameter conforms to Allometric and Boltzmann functions, respectively. The conductivity decreases while the resistivity and DC resistance gradually increase, and the relationship between conductivity, resistivity, DC resistance, and its diameter conforms to the ExpAssoc. ExpAssoc, and Allometric function relation, respectively.

Acknowledgments: This work was supported by the National Natural Science Foundation of China (Grant No. 52071133), National Key Research and Development Program (Grant No. 2016YFB0301400), Key Technologies R & D Program of He'nan Province (Grant No. 202102210207), Chinese Postdoctoral Science Foundation (Grant No. 2020M672222), Henan Innovation Leading Project (Grant No. 191110210400), Innovation Fund for Outstanding Talents of Henan Province (Grant No. 182101510003), and Luoyang Science and Technology Major Project (Grant No. 1901006A).

Conflict of interest: The authors declare no conflict of interest regarding the publication of this paper.

References

[1] Li S, Guo X, Zhang S, Feng J, Song K, Liang S. Arc erosion behavior of TiB_2/Cu composites with single-scale and dual-scale TiB_2 particles. Nanotechnol Rev. 2019;8(1):619–27.
[2] Madhavan R, Pascal B, Robert A. Wear resistance of Cu/Ag multilayers: a microscopic study. ACS Appl Mater Interfaces. 2018;10(17):15288–97.
[3] Li R, Zuo X, Wang E. Influence of thermomechanical process and Fe addition on microstructural evolution and properties of Cu–26 wt% Ag composite. J Alloys Compd. 2019;773:121–30.
[4] Konakov VG, Kurapova OY, Novik NN, Golubev SN, Osipov AV, Graschenko AS, et al. Optimized approach for synthesis of nanotwinned copper with enhanced hardness. Rev Adv Mater Sci. 2014;39(1):1–8.
[5] Zhang X, Zhang Y, Tian B, Song K, Liu P, Jia Y, et al. Review of nano-phase effects in high strength and conductivity copper alloys. Nanotechnol Rev. 2019;8(1):383–95.
[6] Li GM, Wang EG, Zhang L, Zuo X, He J. Research development of deformed processed Cu–Ag *in situ* composites. Mater Rev. 2010;5:80–4.
[7] Neikov OD, Naboychenko SS, Murashova IB. Production of copper and copper alloy powders. Handbook Non-Ferrous Met. Powder. Kiev, Ukraine: Frantsevich Institute for Problems of Materials Science (IPMS). 2019; p. 571–614
[8] Jian CC, Zhang JQ, Ma XC. Cu–Ag alloy for engineering properties and applications based on the LSPR of metal nanoparticles. RSC Adv. 2019;10(22):13277–85.
[9] Wang S, Zhang Y, Yao D. Micro-structure and properties of Cu–0.5 wt% Ag alloy fine wires with severe cold plastic deformation treatment. Mater Res Express. 2018;5(4):127–34.
[10] Wu X, Wang R, Peng C, Feng Y, Cai Z. Influence of hot isostatic pressing and forging on the microstructure and mechanical properties of Cu–3Ag–1Zr alloys. Mater Des. 2019;168:107676.
[11] Chen G, Shen J, Zhu Q, Yao S, Wang C, Zhang P. Tensile deformation and fracture behaviours of cold rolled Cu–3 wt% Ag–0.5 wt% Zr thin sheets with different annealed microstructures. Mater Sci Eng A. 2019;756:27–34.
[12] Li JF. Review of the copper wire bonding technology research and market trend. Non-Ferrous Min Metall. 2015;31(5):60–3.
[13] Jia SG, Zheng MS, Liu P, Ren FZ, Tian BH, Zhou GS, et al. Aging properties studies in a Cu–Ag–Cr Alloy. Mater Sci Eng A. 2006;419(1–2):8–11.
[14] Han K, Vasquez AA, Xin Y, Kalu PN. Microstructure and tensile properties of nanostructured Cu–25 wt% Ag. Acta Mater. 2003;51(3):767–80.
[15] Zhang X, Huang Y, Liu X, Yang L, Shi C, Wu Y, et al. Microstructures and properties of 40Cu/Ag(Invar) composites fabricated by powder metallurgy and subsequent thermo-mechanical treatment. Metall Mater Trans A. 2018;49A(5):1869–78.
[16] Li R, Wang E, Zuo X. Co-precipitation, strength and electrical resistivity of Cu–26 wt% Ag–0.1 wt% Fe alloy. Materials. 2017;10(12):1383.
[17] Kormout KS, Ghosh P, Bachmaier A, Hohenwarter A, Pippan R. Effect of processing temperature on the microstructural characteristics of Cu–Ag nanocomposites: from supersaturation to complete phase decomposition. Acta Mater. 2018;154:33–44.
[18] Arnaud C, Lecouturier F, Mesguich D, Ferreira N, Chevallier G, Estournès C, et al. High strength-high conductivity double-walled carbon nanotube–copper composite wires. Carbon. 2016;96:212–5.
[19] Feng CL, Qin FL, Jie MS, Wu G, Liu G, Li L. Effects of drawing process on properties of directional solidification Cu–Ag conduct wires. Spec Cast Nonferrous Alloys. 2015;8:112–5.
[20] Ning YT, Zhang XH, Zhang J. Stability of heavy deformed Cu–Ag alloy *in situ* filamentary composites. Chin J Nonferrous Met. 2005;4:18–24.
[21] Zhang L, Meng L. Microstructure and mechanical properties of Cu–12%Ag filamentary composite, Chin. J Nonferrous Met. 2005;15(5):751–6.
[22] Zhang L, Meng L. Effect of alloying elements on the microstructure, mechanical properties and electrical properties of Cu–Ag alloy. Chin J of Nonferrous Met. 2002;12(6):1218–23.
[23] Konakov VG, Kurapova OY, Solovyeva EN, Lomakin IV, Archakov IY. Synthesis, structure and mechanical properties of bulk "copper–graphene" composites. Rev Adv Mater Sci. 2018;57:151–7.

[24] Gaolei X, Lijun P, Xujun M, Haofeng X, Guojie H, Zhen Y, et al. Microstructure and properties of Cu–Cr–Ag alloy fabricated by up-drawn continuous casting and continuous extrusion. Rare Met Mater Eng. 2019;48:1310–6.
[25] Simhan DR, Ghosh A. Vacuum brazing of cubic boron nitride to medium carbon steel with Zr added passive and Ti activated eutectic Ag–Cu alloys. Ceram Int. 2017;44(5):4891–9.
[26] Zuo X, Han K, Zhao C, Niu R, Wang E. Microstructure and properties of nanostructured Cu28 wt% Ag microcomposite deformed after solidifying under a high magnetic field. Mater Sci Eng A. 2014;619(12):319–27.
[27] Zhao C, Zuo X, Wang E, Han K. Strength of Cu–28 wt% Ag composite solidified under high magnetic field followed by cold drawing. Met Mater Int. 2017;23(2):369–77.
[28] Liu J, Meng L, Zeng YW. Microstructure evolution and properties of Cu–Ag microcomposites with different Ag content. Mater Sci Eng A. 2006;435(11):237–44.
[29] Moisy F, Gueydan A, Sauvage X, Keller C, Guillet A, Nguyen N, et al. Elaboration of architectured copper clad aluminium composites by a multi-step drawing proces. Mater Sci Forum. 2018;941:1914–9.
[30] Byakovskiy AA, Zheleznyak LM, Yezhov YA. Use of horizontal continuous casting plant for manufacture of various products. Tekhnol Met. 2018;10:44–8.
[31] Yuan D, Yang B, Chen J, Chen H, Zhang J, Wang H. Upward continuous casting in the manufacture of Cu–Cr–Ag alloys: potential for enhancing strength whilst maintaining ductility. Metall Mater Trans A. 2017;48:6083–90.
[32] Han K, Vasquez AA, Xin Y, Kalu PN. Microstructure and tensile properties of nanostructured Cu–25 wt% Ag. Acta Mater. 2003;51(3):767–80.
[33] Zhao H, Fu H, Xie M, Xie J. Effect of Ag content and drawing strain on microstructure and properties of directionally solidified Cu–Ag alloy. Vacuum. 2018;154:190–9.
[34] Zhao J, Deng Y, Tang J, Zhang J. Influence of strain rate on hot deformation behavior and recrystallization behavior under isothermal compression of Al–Zn–Mg–Cu alloy. J Alloys Compd. 2019;809:151788.
[35] Kwon SK, Kim HD, Pei XQ, Ko HE, Park HW, Bennewitz R, et al. Effect of cooling rate on the structure and nanotribology of Ag–Cu nano-eutectic alloys. J Mater Sci. 2019;54(12):9168–84.
[36] Lee KA, Kim SJ, Kim YM, Kim MC. Continuous strip casting, microstructure and performance of Ag–Cu brazing alloy. Solid State Phenom. 2006;116–117:750–3.
[37] Zuo X, Guo R, Zhao C, Zhang L, Wang E, Han K. Microstructure and properties of Cu–6 wt% Ag composite thermomechanical-processed after directionally solidifying with magnetic field. J Alloys Compd. 2016;676:46–53.
[38] Joo HS, Hwang SK, Im YT. Effect of thermomechanical treatment on mechanical and electrical properties of Cu–Cr–Zr alloy in continuous hybrid process. Procedia Manuf. 2018;15:1525–32.
[39] Morozova A, Mishnev R, Belyakov A, Kaibyshev R. Microstructure and properties of fine grained Cu–Cr–Zr alloys after termo-mechanical treatments. Rev Adv Mater Sci. 2018;54(1):56–92.
[40] Tardieu S, Mesguich D, Lonjon A, Lecouturier F, Ferreira N, Chevallier G, et al. Nanostructured 1% silver–copper composite wires with a high tensile strength and a high electrical conductivity. Mater Sci Eng. 2019;761(Jul 22):138048.
[41] Kawecki A, Knych T, Sieja-Smaga E, Mamala A, Kwaśniewski P, Kiesiewicz G, et al. Fabrication, properties and microstructures of high strength and high conductivity copper–silver wires. Arch Metall Mater. 2012;57(4):1261–70.
[42] Zhang X, Zhang Y, Tian B, Jia Y, Liu Y, Song K, et al. Cr effects on the electrical contact properties of the Al_2O_3–Cu/15W composites. Nanotechnol Rev. 2019;8(1):128–35.
[43] Wang M, Beyerlein IJ, Zhang J, Han WZ. Defect-interface interactions in irradiated Cu/Ag nanocomposites. Acta Mater. 2018;160:211–23.
[44] Aramesh S, Doostmohammadi A, Rezai P. Poly(dimethylsiloxane)/Cu/Ag nanocomposites: electrical, thermal, and mechanical properties. Polym Compos. 2019;40(10):4093–101.
[45] Feng J, Liang S, Guo X, Zhang Y, Song K. Electrical conductivity anisotropy of copper matrix composites reinforced with SiC whiskers. Nanotechnol Rev. 2019;8(1):285–92.